ACS APPLIED MATERIALS & INTERFACES

Research Article

www.acsami.org

Fabrication of a $Cu_2ZnSn(S,Se)_4$ Photovoltaic Device by a Low-Toxicity Ethanol Solution Process

Gang Wang, Wangen Zhao, Yong Cui, Qingwen Tian, Shang Gao, Lijian Huang, and Daocheng Pan*

State Key Laboratory of Rare Earth Resource Utilization, Changchun Institute of Applied Chemistry, Chinese Academy of Sciences, 5625 Renmin Street, Changchun, Jilin 130022, China

Supporting Information

ABSTRACT: Homogeneous molecular precursor solutions are excellent choices for obtaining smooth absorber layers, and they offer the potential to significantly lower the manufacturing cost of solar cells. Here, we present a thermally degradable metal butyldithiocarbamate-based solution approach to fabricate $Cu_2ZnSn(S,Se)_4$ solar cells. Low-cost Cu_2O, ZnO, and SnO were used as the starting materials and were dissolved in the ethanol solution of butyldithiocarbamic acid. By tuning the composition of the $Cu_2ZnSn(S,Se)_4$ thin film, a power conversion efficiency of 6.03% on the basis of the active area has been achieved.

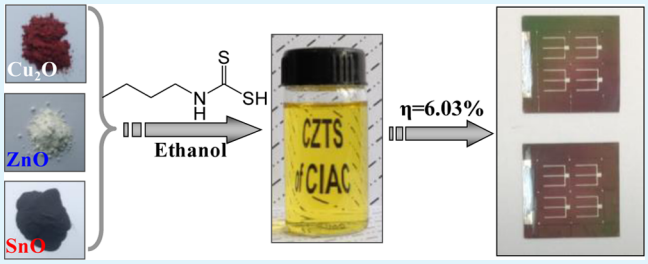

KEYWORDS: *CZTSSe, kesterite, thin film, solar cells, solution process*

INTRODUCTION

Chalcopyrite $Cu(InGa)Se_2$ (CIGSe) thin-film solar cells have demonstrated efficiencies above 20% and have currently reached the industrial production level.[1,2] However, the shortage and high material cost of indium and gallium could limit CIGSe production and lead to a high module price, which impels researchers to seek other alternative photovoltaic materials.[3−5] Recently, kesterite $Cu_2ZnSn(S,Se)_4$ (CZTSSe) compounds have received increasing attention because of their low material cost.[6−10] The kesterite structure of CZTSe is derived from the chalcopyrite crystal structure of CIGSe, where In^{3+} and Ga^{3+} ions are substituted by an equal number of Zn^{2+} and Sn^{4+} ions.[11,12] Compared with CIGSe, $Cu_2ZnSn(S,Se)_4$ compounds also have a suitable direct band gap and a high absorption coefficient, and they are being considered as ideal absorber materials for thin-film solar cells.[6−14]

Various approaches have been reported to fabricate CZTSSe absorber layers, including vacuum-deposition technologies (e.g., thermal coevaporation, sputtering, and pulsed-laser deposition) and non-vacuum-deposition technologies (e.g., electrodeposition and solution process).[3−5] Although the real nature of CZTSSe is not well understood, these thin-film deposition methods have been well investigated and have yielded a dramatic increase in the solar-energy conversion efficiency.[3−5,15−22] For vacuum-deposition technologies, the power conversion efficiencies (PCEs) of 8.4 (by metallic precursor coevaporation)[15] and 9.2% (by four-source coevaporation)[16] have been achieved. For non-vacuum-deposition technologies, some attractive power conversion efficiencies of 7.3 (by metallic precursor electroplating),[17] 4.1 (by a soluble precursor organic solution method),[18] 8.4 (by quaternary nanocrystals ink coating),[19] 8.5 (by binary and ternary nanocrystals coating),[20] and 8.08% (by a hydrazine-based true solution method)[21] have been achieved by several research groups. Recently, a world-record efficiency of 11.1% was reported for CZTSSe solar cells by Mitzi et al. using a hydrazine-based particle-containing slurry method.[22] Compared with vacuum-deposition technologies, non-vacuum-deposition technologies are superior in energy-conversion efficiency and fabrication costs for CZTS solar cells.[3−5,15−22] However, hydrazine-based solutions and nanoparticle-based inks have some limitations for large-scale production because of their toxicity or the complexity of the synthesis; therefore, it is highly desirable to develop a low-toxicity and facile solution method.[3−5] Recently, we reported a novel and versatile metal−organic molecular precursor-based solution approach and successfully fabricated CIGSSe[23] and CISSe[24] solar cells with conversion efficiencies of 8.8 and 10.1%, respectively. Notably, it is a comparatively simple, safe, low-cost, and general molecular precursor-based solution approach. Here, we extended this method to fabricate high-efficiency CZTSSe solar cells and obtained a PCE of 6.03% on the basis of the active area.

EXPERIMENTAL SECTION

Materials. Copper(I) oxide (Cu_2O, 99.99%), zinc oxide (ZnO, 99.99%), and tin(II) oxide (SnO, 99.9%) were purchased from Aldrich. Carbon disulfide (CS_2, 99.9%), 1-butylamine ($CH_3(CH_2)_3NH_2$, 99%), thioglycolic acid ($HSCH_2COOH$, 99%), ethanol (CH_3CH_2OH, AR), selenium (Se, 99.9%), ammonium

Received: July 1, 2013
Accepted: September 20, 2013
Published: September 20, 2013

   dx.doi.org/10.1021/am402558a | ACS Appl. Mater. Interfaces 2013, 5, 10042−10047

hydroxide (NH_4OH, 25%), cadmium sulfate ($CdSO_4$, 99%), and thiourea (NH_2CSNH_2, 99%) were obtained from Aladdin. All chemicals were used as received without any further purification.

Preparation of CZTS Precursor Solution. First, 1.5 mL of ethanol, 1.05 mL of CS_2 (~17.5 mmol), 1.75 mL of 1-butylamine (~17.5 mmol), and 0.4 mL of thioglycolic acid (~5.7 mmol) were mixed in a 25 mL conical flask under magnetic stirring at room temperature. Afterwards, SnO (0.270g, ~2.0 mmol) was loaded into the flask, and the flask was transferred into an ultrasonic water bath at 40 °C for 45 min until all of the solid was dissolved. The Cu and Zn precursor solutions were prepared with a similar procedure except for thioglycolic acid. The Cu precursor solution contained 1.5 mL of ethanol, 1.05 mL of CS_2 (~17.5 mmol), 1.75 mL of 1-butylamine (~17.5 mmol), and 0.215 g of Cu_2O (~1.5 mmol). The Zn precursor solution contained 1.5 mL of ethanol, 0.6 mL of CS_2 (~10 mmol), 1 mL of 1-butylamine (~10 mmol), and 0.187 g of ZnO (~2.3 mmol). Subsequently, the three solutions were mixed together under magnetic stirring to form a light-yellow solution. Finally, the CZTS precursor solution was diluted to a total metal concentration of 0.55 M with ethanol followed by centrifugation at 12 000 rpm for 10 min prior to spin-casting. All of the procedures were conducted in the air.

Deposition of the CZTSSe Absorber Layer and Fabrication of the Solar-Cell Device. The CZTS precursor thin film was spun on a Mo-coated coverslip ($20 \times 20 \times 0.5$ mm^3, with ~1 μm thick Mo) at 3000 rpm for 20 s followed by a sintering process on a 320 °C ceramic hot plate for 1 min to form the CZTS nanocrystal thin film. The CZTS nanocrystal thin film with a thickness of ~1.4 μm was obtained by repeating eight spin-casting/sintering cycles. Subsequently, two films and 30 mg of selenium powder were sealed in a hard test tube (25 mm in diameter and ~30 mL in volume) under vacuum (Figure S1) followed by a selenization process at 540 °C for 45 min in a preheated furnace.[23] The solar-cell device was completed by chemical-bath depositing 60 nm of a CdS thin film (100 mL of deionized H_2O, 12.5 mL of NH_4OH, 50 mL of cadmium sulfate (0.006 M), and 50 mL of thiourea (0.03 M) in a 65 °C water bath for 15 min), RF-sputtering 70 nm of intrinsic ZnO (100 W, 0.4 Pa Ar, 5 min), DC-sputtering 250 nm of indium tin oxide (ITO) (90W, 0.5 Pa Ar, 5 min), and thermally evaporating 2 μm of Al grid electrode (thermal evaporation current of 40A, 5 mP, 2 min). The four devices (an active area of 0.368 cm^2 for each cell, ~90% of total device area) were isolated by mechanical scribing with a tungsten needle.

Characterizations. Thermogravimetric analysis (TGA) was performed on a TGA/DSC 1 STARe (Mettler-Toledo). The thickness of the thin film was measured by a step profiler (Ambios, XP-100). The XRD patterns were recorded using a Bruker D8 X-ray diffractometer. The scanning electron microscope (SEM) images were taken on a Hitachi S-4800 equipped with an energy-dispersive X-ray (EDX) analyzer (Bruker AXS XFlash detector 4010). The sample for EDX measurement was prepared on a glass slide. *C*−*V* curves and impedance spectroscopy were measured with a CHI660B electrochemical workstation under dark conditions. A frequency of 1000 Hz and an ac amplitude of 50 mV were applied for *C*−*V* measurement. Impedance spectroscopy was carried out in the frequency range of 1 Hz to 100 kHz at 50 mV of amplitude and 0 V bias potential. *J*−*V* curves were measured with a Keithley 2400 source meter and a solar simulator (Abet Sun 2000; AM 1.5) by a home-made probe station.[23] The light intensity was calibrated to 100 mW/cm^2 using a Newport optical power meter (model 842-PE). The external quantum efficiency and reflection curves were measured using a Zolix SCS100 QE system equipped with a 150 W xenon light source, a lock-in amplifier, and an integrating sphere.

RESULTS AND DISCUSSION

In our previous work, we reported that many types of metal oxides, hydroxides, acetylacetonates, and so forth, can be easily dissolved in the chloroform solution of butyldithiocarbamic acid (BDCA) to form thermally degradable metal-organic molecular precursor solutions.[23] Because of the high toxicity of chloroform, we used nontoxic ethanol as the solvent. However, SnO has a very low rate of dissolution in the ethanol solution of BDCA. Therefore, thioglycolic acid (TA) was adopted as an auxiliary ligand to enhance the rate of dissolution and the stability of the Sn precursor solution. Note that Cu_2O and ZnO can be readily dissolved in the ethanol solution of BDCA without the aid of TA. Finally, Cu, Zn, and Sn precursor solutions were mixed under magnetic stirring to form an air-stable CZTS precursor solution. The schematic process is shown in Figure 1.

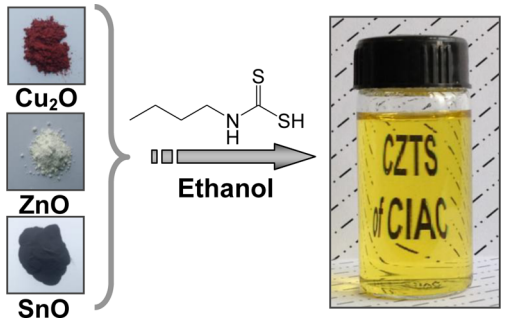

Figure 1. Schematic for preparing the CZTS precursor solution and photograph of a CZTS precursor solution (Cu/(Zn + Sn) ≈ 0.70 and Zn/Sn ≈ 1.15).

Figure 2 presents thermogravimetric analysis (TGA) data for the mixed CZTS precursor (Cu/(Zn + Sn) ≈ 0.70 and Zn/Sn ≈ 1.15). The TGA sample was prepared from the CZTS precursor solution by removal of all low-boiling-point molecules under vacuum at 80 °C followed by heating at 100 °C for 60 min. It was found that these CZTS precursors start to decompose at 150°C, and their weight loss occurs relatively fast between 150 and 250°C. The TGA profile shows that the CZTS precursors are almost completely decomposed at 250 °C. The thermal decomposition mechanism of the metal butyldithiocarbamates has been investigated in detail in the literature, and metal sulfides will form after the thermal decomposition.[25−27]

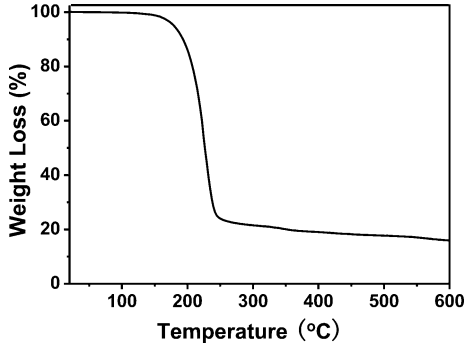

Figure 2. TG curve of the CZTS precursors (Cu/(Zn + Sn) ≈ 0.70 and Zn/Sn ≈ 1.15).

The CZTS precursor solution was used to deposit the CZTS nanocrystal thin film on a Mo-coated sodalime glass (SLG) substrate by a spin-casting process followed by annealing on a 320 °C hot plate for 1 min in a nitrogen-filled glove box. The as-fabricated CZTS thin film was selenized to form a CZTSSe absorber layer under selenium vapor at 540 °C for 45 min in a sealed hard test tube. The crystal structures of as-fabricated CZTS and selenized CZTSSe thin films were examined by

powder X-ray diffraction (XRD), and their XRD patterns are shown in Figure 3a. The as-fabricated CZTS thin film exhibits

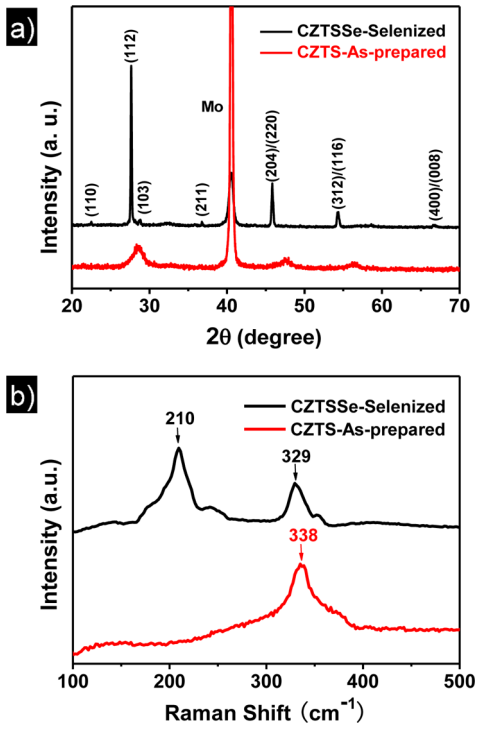

Figure 3. X-ray diffraction patterns (a) and Raman spectra (b) for the as-fabricated CZTS thin film (Cu/(Zn + Sn) ≈ 0.70 and Zn/Sn ≈ 1.15) and the selenized CZTSSe thin film (Cu/(Zn + Sn) ≈ 0.90, Zn/Sn ≈ 1.30, and S/(S + Se) ≈ 0.30).

very broad diffraction peaks (Figure 3a, red line), indicating that the CZTS thin film is composed of small-size nanocrystals. Because the diffraction peaks are weak and broad, the crystal structure of the CZTS nanocrystal thin film is undistinguishable by the XRD pattern. After selenization, the XRD peaks sharpen, indicating that large densely packed grains have been obtained (Figure 3a, black line), which is highly desirable for high-efficiency CZTSSe solar cells. It was observed that the main diffraction peaks shift toward the lower angles after selenization. This is attributed to the expansion of the unit cell volume by the partial replacement of S with Se. The selenized CZTSSe thin film possesses a pure kesterite structure without any impurity phases. In addition, some minor peaks, such as (110), (103), (211), and (400)/(008), become observable after selenization, which demonstrates that the CZTSSe thin film has good crystallinity. As reported in the literature, the incorporation of Se into CZTS can shrink the band gap of CZTSSe, leading to an increase in the short-circuit current.[28,29]

Some binary and ternary sulfides and selenides, such as ZnS, Cu_2SnS_3, ZnSe, and Cu_2SnSe_3, have similar XRD patterns with CZTS and CZTSe; therefore, XRD is insufficient to determine the phase purity of the CZTS and CZTSSe thin films.[30−34] Raman spectroscopy is able to detect possible secondary phases such as Cu_xS, ZnS, SnS, Cu_2SnS_3, and so forth. Therefore, the as-fabricated CZTS and selenized CZTSSe thin films were examined by Raman spectroscopy, as shown in Figure 3b. For the as-fabricated CZTS thin film, the major peaks appear at 338 cm^{-1} (Figure 3b, red line), consistent with previously reported CZTS values,[31,32] indicating that the pure CZTS thin film was obtained by thermal decomposition of metal butyldithiocarbamates at 320 °C without any binary and ternary chalcogenides, including Cu_2S, ZnS, SnS, and Cu_2SnS_3.[31−33] For the selenized CZTSSe thin film, the main peaks are located at 210 and 329 cm^{-1} (Figure 3b, black line), which are in good agreement with the literature results for CZTSSe with S/(S + Se) ≈ 0.30.[21] No possible impurity phases ($Cu_x(S,Se)_y$, Zn(S,Se), Sn(S,Se), and $Cu_2Sn(S,Se)_3$) are found in the Raman spectrum for the selenized CZTSSe thin film.[31−34]

The chemical composition of the CZTSSe thin film is critically important to the performance of the CZTSSe solar cell. Typically, the Cu-poor and Zn-rich CZTSSe absorber layer is highly desirable in a CZTSSe device to avoid the formation of unfavorable Cu_{Zn} antisite that has a negative formation energy.[11,12] Generally, the high-efficiency CZTSSe solar cell can be realized in a wide composition range around Cu/(Zn + Sn) ≈ 0.75−0.95 and Zn/Sn ≈ 1.1−1.4.[3,4,11] The chemical composition of the as-fabricated CZTS thin film is $Cu_{1.50}Zn_{1.15}Sn_{1.0}S_{3.50}$, determined by averaging 10 random spots using energy-dispersive X-ray spectroscopy (EDS) (Figure S2), and the selenized CZTSSe film has a Cu/(Zn + Sn) ratio of 0.90 and a Zn/Sn ratio of 1.30, which are slightly different from those of the starting CZTS thin film and are consistent with those previously reported for high-efficiency CZTSSe devices.[11,16−22] The Cu/(Zn + Sn) ratio significantly increases after the selenization, and this may be attributed to the seed growth of Cu-rich CZTS nanoparticles. In addition, the ratio of S/(S + Se) is approximately 0.30, which is close to the optimal S/(S + Se) ratio reported by Mitzi et al., indicating that a suitable band gap is obtained.[6] For the fabrication of CZTSSe solar cells, a Cu/(Zn + Sn) ratio of 0.90, a Zn/Sn ratio of 1.30, and a S/(S + Se) ratio of 0.3 were chosen, similar to those of previously reported for record CZTSSe devices.[22]

A representative cross-sectional scanning electron microscope (SEM) image of an as-prepared CZTS thin film on Mo-coated SLG is shown in Figure 4a. A uniform, crack-free, and pinhole-free CZTS nanocrystal thin film with a thickness of ~1.4 μm was formed by a consecutive spin-casting process. Figure 4b,c shows the SEM plane-views of the selenized CZTSSe thin film at different magnifications. After the selenization at 540 °C for 45 min, the CZTSSe thin film has

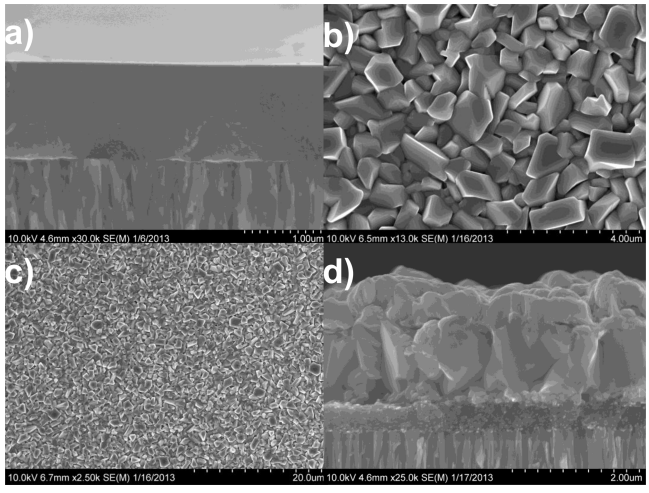

Figure 4. Cross-sectional SEM image of the as-fabricated CZTS nanocrystal thin film on Mo-coated SLG substrate (a). Plane-views of the selenized CZTSSe thin film (b, c). Cross-sectional SEM image of a completed CZTSSe thin-film solar cell (d).

a grain size range from 1 to 2 μm. A cross-sectional SEM image of a completed CZTSSe solar cell is shown in Figure 4d. The selenized CZTSSe thin film exhibits an obvious tri-layer morphology consisting of a dense large-grained top layer of about 1 μm, a medium-grained middle layer of about 200 nm, and a carbon-rich 400 nm small-grained bottom layer near the Mo interface as well as a $MoSe_2$ layer of about 200 nm in thickness. The similar carbon-rich small-grained layer has been observed by various groups for CZTSSe solar cells fabricated by a nanocrystals-based ink process,[19,20] perhaps resulting from some nondecomposed organic molecules being retained in the CZTS film. Interestingly, the thickness of the small-grained layer remains unchanged even when more aggressive selenization conditions are used. Note that the sintering temperature of the CZTS nanocrystal thin film strongly impacts the grain growth of the CZTSSe thin film. When the sintering temperature is above 350 °C, the poor grain growth of CZTSSe will be observed after selenization (Figure S3). Future work will be focused on the crystal-growth mechanism of CZTSSe thin film.

The CZTSSe solar-cell device was fabricated according to the conventional configuration of glass/Mo/CZTSSe/CdS/*i*-ZnO/ITO/Al. The current density−voltage (J−V) curves for a typical CZTSSe solar cell measured in the dark and under AM 1.5 illumination are shown in Figure 5a. The as-fabricated

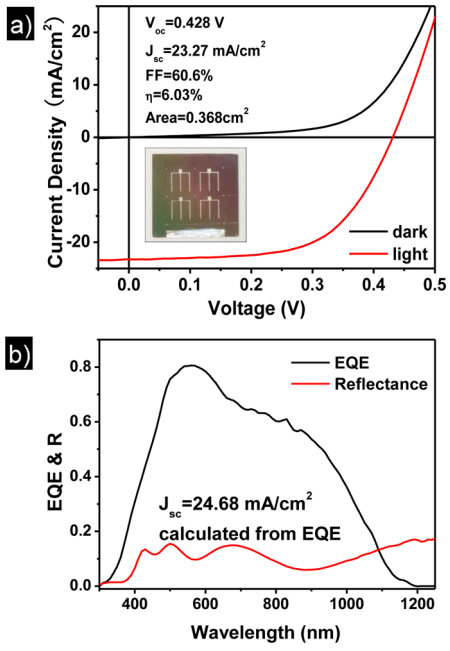

Figure 5. J−V curves of one of the CZTSSe (Cu/(Zn + Sn) ≈ 0.90 and Zn/Sn ≈ 1.30) solar cells measured in the dark and under AM 1.5 illumination (a). The inset shows a digital photograph of the CZTSSe solar cell. External quantum efficiency (EQE) and reflectance spectra of the corresponding CZTSSe solar cell (b).

device exhibits a PCE of 6.03% on the basis of the active area of 0.368 cm^2 (V_{oc} = 0.428 V, J_{sc} = 23.27 mA/cm^2, and FF = 60.6%). Our J_{sc} is significantly lower than those of high-efficiency CZTSSe solar cells in the literature.[16−22] The J_{sc} losses are analyzed by measuring the external quantum efficiency (EQE) and reflectance spectra, as shown in Figure 5b. First, the band gap of CZTSSe absorber layer was calculated to be 1.2 eV by EQE spectrum (Figure S4), which is somewhat higher than those reported for high-efficiency CZTSSe solar cells (~1.15 eV).[6−10,16−22] Second, the highest quantum efficiency in the visible-light range is only 80% because of a relatively high reflectivity of ~11.4% in the range of 400−1200 nm. It is expected that a significant improvement in device performance should be achieved by depositing a MgF_2 antireflection film.[16−22,35] The calculated J_{sc} from the EQE spectrum is 24.68 mA/cm^2, which is slightly higher than the measured J_{sc} under AM 1.5 illumination. Additionally, the overall PCE is limited owing to a carbon-rich small-grained layer and undesirable impurity phases between the large-grained layer and Mo substrate, resulting in a high series resistance and a substantial decrease in current density.[19,20] The medium-grained middle layer in the current CZTSSe thin film with tri-layer morphology may seriously limit the efficiency of solar cells, which can restrict the transport of photo-generated carriers and form grain-boundary recombination.

J−V analysis was used to determine the diode parameters of CZTSSe solar cell according to the literature method, and the dark and light J−V curves were redrawn in three successive plots (Figure 6).[36] First, the dark and light shunt conductanes (G) were calculated to be 3.2 and 2.6 mS/cm^2 by a plot of dJ/dV versus V in Figure 6a. The shunt conductance is higher than

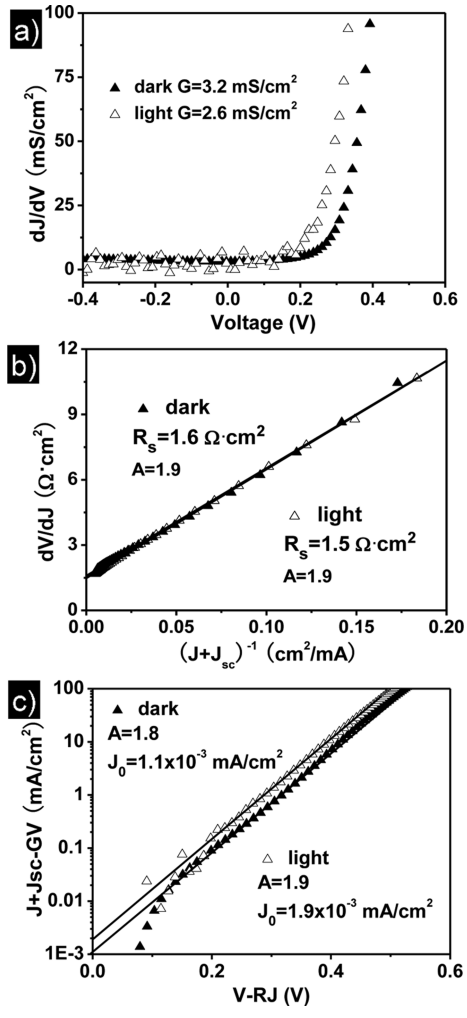

Figure 6. Plots of dJ/dV vs V redrawn from the standard dark and light J−V curves (a). Plots of dV/dJ vs $(J + J_{sc})^{-1}$ (b). Semi-logarithmic plots of $J + J_{sc}$−GV vs V−RJ; J_0 was obtained by the intercept of the linear region of the curves, and the slope is equal to q/AkT (c).

those of high-efficiency CIGS solar cells (<1 mS/cm^2).[36] Figure 6b shows $r(J)$ curves ($r(J) \equiv dV/dJ$ vs $(J + J_{sc})^{-1}$) for the same CZTSSe device. The series resistance (R_s) is around 1.5 to 1.6 Ω cm^2, and the diode quality factor (A) is 1.9. These values are somewhat larger than those reported by Mitzi et al. for the best CZTSSe solar cells.[22] It was inferred that the 6.03% efficiency CZTSSe device suffered from high a R_s value, which was caused by the carbon-rich small-grained layer and unavoidable impurity phases between the CZTSSe large-grained layer and Mo layer. Finally, Figure 6c shows two semi-logarithmic plots of $J + J_{sc}-GV$ versus $V-RJ$. The intercept for the dark data gives the reverse saturation current density $J_0 = 1.1 \times 10^{-3}$ mA/cm^2, and the slope gives $A = 1.8$, in good agreement with the value obtained from Figure 6b. Note that a large A value and a high reverse saturation current density will lower the V_{oc} and FF values of the solar cell.

The $C-V$ and $1/C^2-V$ curves of the CZTSSe solar cell are shown in Figure 7a for determining the effective hole concentration of the CZTSSe absorber layer. Using the Mott–Schottky method, the net carrier concentration can be calculated by the following equation: $N = (2/qk_s\varepsilon_o A^2)\, dV/d(1/C^2)$, where N is the net carrier concentration, q is the electron charge, k_s is the semiconductor dielectric constant, ε_o is the permittivity of free space, A is the area of the solar cell, C is the capacitance, and V is the applied voltage.[37] The calculated carrier concentration of the CZTSSe device is 1.06×10^{16} cm^{-3}, which is close to the value of 2×10^{16} cm^{-3} for a high-efficiency CIGS device.[37] An electrochemical impedance spectroscopy (EIS) measurement was performed on a completed CZTSSe cell. The Nyquist plot and tested ac response equivalent circuit of the CZTSSe solar cell are shown in Figure 7b.[38] The values of R_s and R_{sh} obtained by fitting the spectrum in Figure 7b with a Zview 2.0 program are 2.7 and 459.2 Ω cm^2, respectively, consistent with those of the photocurrent–voltage analysis. The large R_s value of the as-prepared CZTSSe device can be attributed to the presence of the carbon-rich small-grained layer and unavoidable impurity phases between the CZTSSe large-grained layer and Mo layer, although the carbon-rich small-grained layer was not electrically insulating in this case. By reducing the thickness of carbon-rich small-grained layer and eliminating undesirable impurity phases, and thereby reducing R_s, a further increase in the performance of CZTSSe solar cells may be enabled.

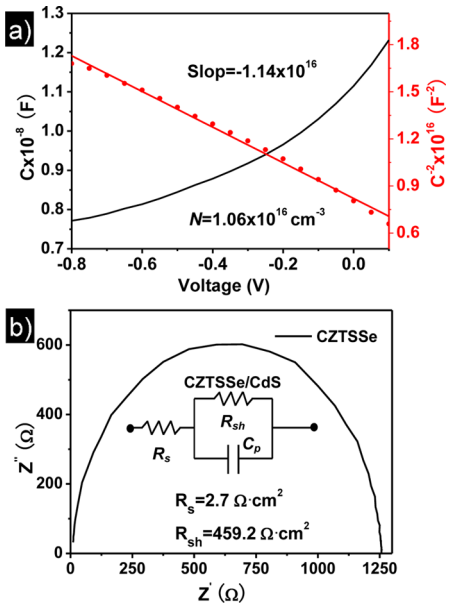

Figure 7. $C-V$ and $1/C^2-V$ curves of the CZTSSe solar cell (a). Nyquist plot and an equivalent circuit (inset) of the CZTSSe solar cell (b).

CONCLUSIONS

A crack- and pinhole-free CZTS nanocrystal thin film has been directly prepared by a low-toxicity ethanol solution method, and a high-quality CZTSSe absorber layer was obtained by selenization. A power conversion efficiency of 6.03% on the basis of the active area has been achieved. The PCE could be further enhanced by the optimization of selenization conditions and the deposition of a MgF_2 anti-reflection layer. Moreover, this solution approach could be extended to produce other earth-abundant $Cu_2MSn(S,Se)_4$ (M = Fe^{2+}, Co^{2+}, Ni^{2+}, and Mn^{2+}) thin-film solar cells.

ASSOCIATED CONTENT

Supporting Information

EDS spectra, chemical compositions, SEM image, and the band gap of the CZTSSe thin film. This material is available free of charge via the Internet at http://pubs.acs.org.

AUTHOR INFORMATION

Corresponding Author

*E-mail: pan@ciac.jl.cn.

Notes

The authors declare no competing financial interest.

ACKNOWLEDGMENTS

This work was supported by the National Natural Science Foundation of China (grant nos. 21071142, 51172229, 51202241, and 51302258).

REFERENCES

(1) Jackson, P.; Hariskos, D.; Lotter, E.; Paetel, S.; Wuerz, R.; Menner, R.; Wischmann, W.; Powalla, M. *Prog. Photovoltaics* **2011**, *19*, 894–897.
(2) Guo, W.; Liu, B. *ACS Appl. Mater. Interfaces* **2012**, *4*, 7036–7042.
(3) Mitzi, D. B.; Gunawan, O.; Todorov, T. K.; Wang, K.; Guha, S. *Sol. Energy Mater. Sol. Cells* **2011**, *95*, 1421–1436.
(4) Ramasamy, K.; Malik, M. A.; O'Brien, P. *Chem. Commun.* **2012**, *48*, 5703–5714.
(5) Katagiri, H.; Jimbo, K.; Maw, W. S.; Oishi, K.; Yamazaki, M.; Araki, H.; Takeuchi, A. *Thin Solid Films* **2009**, *517*, 2455–2460.
(6) Todorov, T. K.; Reuter, K. B.; Mitzi, D. B. *Adv. Mater.* **2010**, *22*, E156–E159.
(7) Guo, Q.; Ford, G. M.; Yang, W.; Walker, B. C.; Stach, E. A.; Hillhouse, H. W.; Agrawal, R. *J. Am. Chem. Soc.* **2010**, *132*, 17384–17386.
(8) Steinhagen, C.; Panthani, M. G.; Akhavan, V.; Goodfellow, B.; Koo, B.; Korgel, B. A. *J. Am. Chem. Soc.* **2009**, *131*, 12554–12555.
(9) Fairbrother, A.; García-Hemme, E.; Izquierdo-Roca, V.; Fontané, X.; Pulgarín-Agudelo, F. A.; Vigil-Galán, O.; Pérez-Rodríguez, A.; Saucedo, E. *J. Am. Chem. Soc.* **2012**, *134*, 8018–8021.
(10) Cho, J. W.; Ismail, A.; Park, S. J.; Kim, W.; Yoon, S.; Min, B. K. *ACS Appl. Mater. Interfaces* **2013**, *5*, 4162–4165.
(11) Chen, S.; Walsh, A.; Gong, X.; Wei, S. *Adv. Mater.* **2013**, *25*, 1522–1539.
(12) Walsh, A.; Chen, S.; Wei, S.; Gong, X. *Adv. Energy Mater.* **2012**, *2*, 400–409.
(13) Bag, S.; Gunawan, O.; Gokmen, T.; Zhu, Y.; Todorov, T. K.; Mitzi, D. B. *Energy Environ. Sci.* **2012**, *5*, 7060–7065.

(14) Woo, K.; Kim, Y.; Moon, J. *Energy Environ. Sci.* **2012**, *5*, 5340−5345.
(15) Shin, B.; Gunawan, O.; Zhu, Y.; Bojarczuk, N. A.; Chey, S. J.; Guha, S. *Prog. Photovoltaics* **2013**, *21*, 72−76.
(16) Repins, I.; Beall, C.; Vora, N.; DeHart, C.; Kuciauskas, D.; Dippo, P.; To, B.; Mann, J.; Hsu, W.; Goodrich, A.; Noufi, R. *Sol. Energy Mater. Sol. Cells* **2012**, *101*, 154−159.
(17) Ahmed, S.; Reuter, K. B.; Gunawan, O.; Guo, L.; Romankiw, L. T.; Deligianni, H. *Adv. Energy Mater.* **2012**, *2*, 253−259.
(18) Ki, W.; Hillhouse, H. W. *Adv. Energy Mater.* **2011**, *1*, 732−735.
(19) Guo, Q.; Ford, G. M.; Yang, W.; Hages, C. J.; Hillhouse, H. W.; Agrawal, R. *Sol. Energy Mater. Sol. Cells* **2012**, *105*, 132−136.
(20) Cao, Y.; Denny, M. S., Jr.; Caspar, J. V.; Farneth, W. E.; Guo, Q.; Ionkin, A. S.; Johnson, L. K.; Lu, M.; Malajovich, I.; Radu, D.; Rosenfeld, H. D.; Choudhury, K. R.; Wu, W. *J. Am. Chem. Soc.* **2012**, *134*, 15644−15647.
(21) Yang, W.; Duan, H.; Bob, B.; Zhou, H.; Lei, B.; Chung, C.; Li, S.; Hou, W. W.; Yang, Y. *Adv. Mater.* **2012**, *24*, 6323−6329.
(22) Todorov, T. K.; Tang, J.; Bag, S.; Gunawan, O.; Gokmen, T.; Zhu, Y.; Mitzi, D. B. *Adv. Energy Mater.* **2013**, *3*, 34−38.
(23) Wang, G.; Wang, S.; Cui, Y.; Pan, D. *Chem. Mater.* **2012**, *24*, 3993−3997.
(24) Zhao, W.; Cui, Y.; Pan, D. *Energy Technol.* **2013**, *1*, 131−134.
(25) Jung, Y. K.; Kim, J.; Lee, J. *J. Am. Chem. Soc.* **2010**, *132*, 178−184.
(26) Alam, N.; Hill, M. S.; Kociok-Köhn, G.; Zeller, M.; Mazhar, M.; Molloy, K. C. *Chem. Mater.* **2008**, *20*, 6157−6162.
(27) Chesman, A. S. R.; Embden, J.; Duffy, N. W.; Webster, N. A. S.; Jasieniak, J. J. *Cryst. Growth Des.* **2013**, *13*, 1712−1720.
(28) Sun, Y.; Zhang, Y.; Wang, H.; Xie, M.; Zong, K.; Zheng, H.; Shu, Y.; Liu, J.; Yan, H.; Zhu, M.; Lau, W. *J. Mater. Chem. A* **2013**, *1*, 6880−6887.
(29) Duan, H.; Yang, W.; Bob, B.; Hsu, C.; Lei, B.; Yang, Y. *Adv. Funct. Mater.* **2013**, *23*, 1466−1471.
(30) Chalapathy, R. B. V.; Jung, G. S.; Ahn, B. T. *Sol. Energy Mater. Sol. Cells* **2011**, *95*, 3216−3221.
(31) Scragg, J. J.; Ericson, T.; Fontané, X.; Izquierdo-Roca, V.; Pérez-Rodríguez, A.; Kubart, T.; Edoff, M.; Platzer-Björkman, C. *Prog. Photovoltaics* 2012, DOI: 10.1002/pip.2265. Accessed July 15th, 2012.
(32) Wang, K.; Gunawan, O.; Todorov, T.; Shin, B.; Chey, S. J.; Bojarczuk, N. A.; Mitzi, D.; Guha, S. *Appl. Phys. Lett.* **2010**, *97*, 143508-1−143508-3.
(33) Guo, L.; Zhu, Y.; Gunawan, O.; Gokmen, T.; Deline, V. R.; Ahmed, S.; Romankiw, L. T.; Deligianni, H. *Prog. Photovoltaics*. DOI: 10.1002/pip.2332. Published Online: Jan 7, 2013 (accessed Feb 2, 2013).
(34) Wang, K.; Shin, B.; Reuter, K. B.; Todorov, T.; Mitzi, D. B.; Guha, S. *Appl. Phys. Lett.* **2011**, *98*, 051912-1−051912-3.
(35) Barkhouse, D. A. R.; Gunawan, O.; Gokmen, T.; Todorov, T. K.; Mitzi, D. B. *Prog. Photovoltaics* **2012**, *20*, 6−11.
(36) Hegedus, S. S.; Shafarman, W. N. *Prog. Photovoltaics* **2004**, *12*, 155−176.
(37) Cho, A.; Ahn, S.; Yun, J. H.; Gwak, J.; Song, J.; Yoon, K. *J. Mater. Chem.* **2012**, *22*, 17893−17899.
(38) Fernandes, P. A.; Sartori, A. F.; Salomé, P. M. P.; Malaquias, J.; Cunha, A. F.; Graca, M. P. F.; González, J. C. *Appl. Phys. Lett.* **2012**, *100*, 233504-1−233504-4.